Understanding the Independent and Inter-dependent Role of Water and Oxidation on the Tribology of Ultrathin Molybdenum Disulfide (MoS_2)

Taib Arif[1,§], Shwetank Yadav[2,§], Guillaume Colas[3], Chandra Veer Singh[1,2*], Tobin Filleter[1*]

[1]Department of Mechanical and Industrial Engineering, University of Toronto, Canada

[2]Department of Materials Science and Engineering, University of Toronto, Canada

[3]FEMTO-STinstitute, Department of Applied Mechanics, Université Bourgogne Franche Comté, CNRS, 24 Chemin de l'Epitaphe , 25000 Besançon, France

Corresponding Authors E-mail*: filleter@mie.utoronto.ca, chandraveer.singh@utoronto.ca

Keywords: Nanotribology, MoS_2, Oxidized-MoS_2, Friction, DFT

Abstract

In this work, the tribological behavior of ultrathin-MoS_2 was investigated to understand the independent roles of water and oxidation. Water adsorption was identified as the primary interfacial mechanism for both SiO_2/pristine-MoS_2 and SiO_2/graphene interfaces, however, tribological behavior of pristine-MoS_2 was observed to be more sensitive to presence of water due to stronger MoS_2-water interaction. Comparison of pristine-MoS_2 and oxidized-MoS_2 revealed that the oxidation of MoS_2 significantly increased its friction and sensitivity to water by play a more detrimental role. The specific effect of oxygen on friction via chemical interactions was studied in isolation through density functional theory (DFT) simulations of a tip sliding on MoS_2 basal planes and over edges before and after oxidation. The maximum change in energy, or energy barrier correlating with friction, as the tip moved across the surface, increased after oxidation by up to 66% for the basal plane and by 25% at the edge. Charge density analysis suggests that the more localized and non-uniform interfacial charge distribution on oxygen rich surfaces, as compared to pristine surfaces, leads to higher resistance to sliding. This confirms that oxygen presence alone increases friction and when coupled with the presence of water, both effects are additive in increasing friction.

Introduction

Billions of dollars are wasted annually due to energy loss caused by friction[1], where energy is dissipated primarily as heat.[2,3] To decrease friction on sliding contacts, microscale-MoS_2 and graphite are widely used solid lubricants for space[4,5] (joints, bearings *etc.*) and aerospace[6] (gears, reaction wheels *etc.*) applications. Though both of the materials consist of weakly interacting layered structures (2D-MoS_2 and graphene), they display a contrary dependence on the humidity at the microscale, where the coefficient of friction (COF) is reported to drop for graphite in the presence of water, yet increases for microscale-MoS_2 coatings.[7–10] In the case of MoS_2, the widely accepted mechanism for the increase in COF is the oxidation of microscale-MoS_2 to the less lubricious MoO_3 from exposure to humidity[11]. However, separating the effect of the unreacted water molecules present and oxidation is difficult in microscale studies. Furthermore, the sensitivity of microscale-MoS_2 to water can be influenced by the structure (amorphous/crystalline) of MoS_2[12] and alloying elements.[13,14] Oxidation thickness of microscale-MoS_2 is reported to be thinner and on the surface with less oxygen penetration within the coating when MoS_2 layers are highly ordered as compared to amorphous.[11] While there is some understanding of mechanisms (localized interlayer shearing, puckering effect, electron phonon coupling *etc.*) at the nanoscale associated with water influencing friction for graphene, graphene oxide (GO) and graphite edges[15–24], there is only limited understanding for MoS_2 and oxidized-MoS_2 at the nano/molecular scale. Advancement of technological tools such as the atomic force microscope (AFM) has allowed studying the fundamental mechanisms governing friction at atomic/molecular scale.[17,18,25,26] In particular, recent advancements for controlling the environment locally around the single AFM contact have expanded our understanding, by moving away from studying friction as a function of normal load only to consider the role of other variables such as relative humidity[15] and temperature.[27,28]

At the atomic scale, MoS_2 is categorized as a 2D transition metal dichalcogenide (TMD), consisting of a covalently bonded tri-layer structure, with molybdenum atoms sandwiched between sulfur atoms.[29] In vacuum, a friction study between 2D-MoS_2/2D-MoS_2 has demonstrated superlubricity, with a COF on the order of 10^{-4} due to incommensurability.[30] Humidity has been shown to increase the coefficient of friction and interlayer shear strength of MoS_2 in contact with a sharp Si_3N_4 AFM tip, however the study neglected to separate the influence of water and oxidation, did not account for the change in geometry of the sharp tip or the substrate effect, and did not identify the underlying mechanisms (specifically, the effect of water molecules vs. oxidation).[31,32] 2D-MoS_2 deposited on few layers of water was found to exhibit elevated vibrational energy resulting in an increase of friction.[33] A similar mechanism of phonon excitation has been reported to increase friction for graphene by similarly suspending graphene on water.[34] The interaction of water molecules is relatively weak with the basal plane of 2D-MoS_2 but they can interact strongly at defects and edges, where oxidation is understood to initiate.[35,36] Though the literature generally agrees that the oxidized state of MoS_2 as MoO_3 at the microscale is detrimental to its lubricious behavior, recent studies have questioned this frictional behavior of oxidized 2D-MoS_2.[37,38] For instance, theoretical DFT simulations have reported easier shearing between 2D-MoS_2/2D-MoO_3 than 2D-MoS_2/2D-MoS_2. Additionally, Chow et al. reported that the substitution of sulfur atoms with oxygen atoms can change the wettability of monolayer 2D-MoS_2.[39] While wettability has been shown to influence the friction behavior on other 2D materials, it has not been studied for 2D-MoS_2.[15] Therefore, there is a need for studying the influence of water and oxidation on MoS_2 to better understand how they can improve or degrade frictional behavior, while also conducting complementary atomistic simulations for further insights on the mechanisms. Such fundamental understanding will be of great importance in particular for space applications where MoS_2 coating already undergo extensive testing ensuring its durability.

In this work, we study the independent and inter-dependent role of water and oxidation on the tribological behavior of ultrathin-MoS_2 (few layers of 2D-MoS_2). In particular, the behavior of pristine ultrathin-MoS_2 is compared with our previous studies on ultrathin-graphene[15] to provide insight into the role of water. Furthermore, the influence of oxidation on ultrathin-MoS_2 was studied using a combined experimental and computational approach by comparing the tribological behaviour of pristine ultrathin-MoS_2 and oxidized ultrathin-MoS_2 at varying humidity to deconvolute the role of water before and after oxidation. Density functional theory (DFT) simulations were used to gain further insight into the electron charge interactions for both pristine and oxidized MoS_2 on basal planes and step edges for deconvoluting the role of water and oxidation.

Results and Discussion

Water adsorption and oxidation of ultrathin-MoS_2

Figure 1a shows the change in thickness by tapping mode AFM imaging of pristine ultrathin-MoS_2 while varying the humidity and comparing the behavior to that of ultrathin-graphene. The thickness was normalized (Figure 1 - y_{axis}) by dividing the current thickness (H_i) at a given humidity with the thickness at *RH*5% ($H_{RH5\%}$) for pristine-MoS_2. Pristine-MoS_2 of approximately 5 layers (~3.3nm) was exposed to varying humidity from *RH*5% to *RH*75%. It was observed that the increase in humidity had no influence on topography and minimal effect on the change in thickness of ~0.4nm (~12% increase in thickness) for MoS_2 (Figure 1b). This behavior of pristine-MoS_2 was observed to be similar to graphene, and contrary to the large increase in thickness previously reported for graphene oxide.[15] This is consistent with previous reports that water intercalating between the MoS_2/substrate requires very long exposure time (weeks) at extremely high humidity (+*RH*95%).[33,34] Furthermore, the atomic structure of pristine-MoS_2 also prevents water from intercalating between the layers due to the small interlayer distance, the lack of strong interlayer bonding sites for the water molecules and native oxides at the

edges.[15,40] Both pristine-MoS_2 and graphene physically interact with water at the basal plane[35] and recent studies have suggested the formation of ice like water on the basal plane of other 2D materials.[41] Therefore the small increase in thickness of pristine-MoS_2 by ~0.4nm is attributed to a single layer of water adsorbing on the pristine-MoS_2 surface.[33]

X-ray photoelectron spectroscopy (XPS) reveals the presence of 3.9at% of oxygen in the un-annealed pristine-MoS_2 sample (Figure 1c). The oxygen measured is expected as the highly reactive edges/defects can substitute sulfur atoms with environmental oxygen atoms to form native edge oxides. This behavior was further supported by our DFT results, which showed that oxidation of pristine-MoS_2 edges through substitution of sulfur atoms is highly energetically favorable (Figure 1d). To further oxidize MoS_2, samples were annealed in air at 290°C for 3hrs. XPS confirmed the increase in oxygen from 3.9at% to 9.6at% (Figure 1c). High-resolution XPS shows an increase in the intensity of the O1s peak (Figure 1c) as well as some broadening of the $Mo3d_3$ peak at 232.2eV and the initiation of a new $Mo3d_{3/2}$ peak at 235.4eV, indicating the formation of MoO_3 structure post-annealing (Supporting information; Figure S1). Annealing is also expected to increase the coverage of oxygen along the basal plane of MoS_2 in addition to at the edges/defect sites.[11]

Role of water on friction of pristine ultrathin MoS_2

The friction and adhesion behavior of pristine ultrathin-MoS_2 was investigated as a function of humidity and compared to that of ultrathin-graphene (Figure 2) using a custom SiO_2 beaded AFM cantilever. It was observed that the increase in humidity increased the overall friction force for the SiO_2/ pristine-MoS_2 interface from ~1.7±0.1nN (*RH*3%) to ~8.9±0.2nN (*RH*65%). Comparing the behavior of pristine-MoS_2 with graphene, both the materials experienced an overall increase in friction force with the presence of water. Though the general increasing friction trends are similar for both the 2D materials, it is interesting to highlight that the friction transitions at lower humidity for pristine-MoS_2 as compared

to graphene. For pristine-MoS_2, increase in friction occurs at humidity as low as *RH*20% while for graphene at *RH*50% (Figure 2a – grey and black arrows). This behavior was repeatable for two different sample datasets and for varying normal loads (Supporting information; Figure S2). Adhesion between the SiO_2/pristine-MoS_2 interface was determined by measuring the pull off force and was found to increase from ~943±8nN (*RH*10%) to ~1495±143nN (*RH*45%) for the first data set and from ~530±14nN (*RH*10%) to ~1180±14nN (*RH*60%) for the subsequent dataset. The overall adhesion between the SiO_2/pristine-MoS_2 interface was observed to be higher than SiO_2/graphene. The adhesion and friction trends overlapped for pristine-MoS_2 and are observed to increase at *RH*20%, indicating that adhesion plays a significant role in defining the friction behavior for pristine-MoS_2. From the previous section (Figure 1), it was concluded that both pristine-MoS_2 and graphene have similar water adsorption behavior, where both the materials physisorb a single layer of water on the top surface. Herein, both the materials show overlapping friction-adhesion trends (Figure 2) indicating water adsorption as the primary mechanism dictating their tribological behavior at the atomic scale. This was further supported as a similar behavior of pristine-MoS_2 was also observed for sliding against a sharp diamond tip (Supporting information; Figure S3). To understand the difference in sensitivity to water between pristine-MoS_2 and graphene, it is important to highlight their differences in interaction with water.

MoS_2 has a tri-layer atomic structure, where the Mo/S atoms can polarize more strongly than the monolayer carbon structure of graphene to physisorb water on to the surface.[35] The absorption energy of a water molecule on defect free monolayer MoS_2 is reported to be -0.18eV compared to -0.15eV on graphene.[35] The adsorption energy is reported to further increase for thicker and defective MoS_2.[35] Water contact angle (WCA) measurements show a lower contact angle of ~80 on pristine-MoS_2 as compared to ~91°on graphene (Supporting information; Figure S4). In addition, the water slip length on respective surfaces has been reported to be lower on MoS_2 (~1.8nm) compared to that on graphene (~12nm).[42–45] The slip length is the distance between solid (2D material)/liquid(water) interface and the

velocity profile extrapolated to zero.[45] It is used as an indicator to give an insight on the relative ease of water mobility and energy dissipation on a solid surfaces. The lower slip length on MoS_2 basal plane suggests more difficult water slippage resulting in higher viscous interfacial force experienced by the sliding counter surface. This is also consistent with the recent atomistic simulations and theoretical calculations which predict that the COF between water/MoS_2 to be higher than between water/graphene[44,46], hence influencing the energy dissipation mechanism of interlayer shearing as a result of the newly evolved interface from water adsorption. Therefore, it is the atomic structure of MoS_2 which makes it more sensitive to water at lower humidity of *RH*20%.

Role of oxidation on friction of ultrathin MoS_2

This section compares the tribological behavior of pristine ultrathin-MoS_2 and oxidized ultrathin-MoS_2 as a function of humidity using the same SiO_2 beaded tip. The average friction force on oxidized-MoS_2 (Figure 3) was observed to be significantly higher as compared to that of pristine-MoS_2 at any given humidity, with friction increasing from 27±1.3nN (*RH*3%) to 145nN±8nN (*RH*70%). This behavior was repeatable for two different sample datasets and for varying normal loads (Supporting information; Figure S5). The less lubricious behavior of oxidized-MoS_2 is consistent with oxidized microscale-MoS_2 behavior.[11] Adhesion measurements between SiO_2/oxidized-MoS_2 show some increase between *RH*3% (679nN) and *RH*11% (842nN) and plateaus with further increase in humidity. Unlike the behavior of SiO_2/pristine-MoS_2 observed earlier (Figure2), friction and adhesion trends do not correlate well for SiO_2/oxidized-MoS_2. A large increase in friction initiates around 30% humidity, however, minimal change in adhesion between 11–70% suggests that adhesion does not play as important a role in the oxidized-MoS_2 case. Interestingly, oxidized-MoS_2 was found to be more sensitive to water, with friction increasing at even lower humidity of *RH*11%, compared to the *RH*20% for pristine-MoS_2. Chow et al reported MoS_2 to be more hydrophilic once sulfur atoms are substituted with oxygen atoms.[47] Therefore

water is seen to play a much more detrimental role on the tribology of MoS_2 contacts once some oxidation has initiated, particularly along the basal plane.

To further investigate the effect of oxidization on friction for MoS_2, DFT simulations were conducted to characterize the surface interaction of a diamond tip as it moved across pristine and oxidized MoS_2 basal planes and step edges. The change in the potential energy surface shape, specifically its corrugation, with changes in relative position of interacting surfaces as they slide past one another is directly correlated with the resistance to sliding and hence the friction force.[48,49] The larger the energy change with position, in effect an energy barrier, the greater will be the friction force. Hence, we tracked system energy as the diamond tip was translated across a particular surface in fixed distance increments and plotted the changes in system energy with regards to distance travelled to identify which surfaces produced higher friction force (Figure 4).

For the basal planes, random surface layer sulfur atoms were substituted with oxygen in increasing proportions of 30%, 45% and 60% oxygen coverage corresponding to 9.7, 15.3 and 19.4 at% of total oxygen for the MoS_2 material system. The XPS result earlier (Figure 1c) showed similar range of oxidation after annealing with 9.6 at% oxygen corresponding to the 30% oxygen coverage DFT case. Figure 4a shows the absolute energy change of the system with regards to the energy of the initial configuration. The overall trend was that higher oxygen content produced higher relative energy changes, especially in terms of the maximum change (Table 1). The random distribution of oxygen, different for each surface, would account for why the trend isn't always present at every point along the path (Figure 4b-c).

The step edge displayed the same trend with the native oxidized edge (where the maximum possible oxygen substitution leads to MoO_3 units at the edge[50] and is very energetically favorable) showing greater change in interaction energy than the pristine step edge (Figure 4d-f). Figure 4d shows the system

energy relative to the starting position, whether higher or lower, in order to capture the effect of going over the edge. The barrier that is visible in the energy profile as a sharp peak and drop-off, when the tip approaches the step edge at around 33 Å, is often referred to as the Schwoebel barrier/effect and is also observed for graphene.[51] For the native oxidized edge, this barrier was found to be ~ 25% higher than for the pristine edge which further confirms that oxidation increases friction. The maximum energy change for either case is also significantly higher than for any basal plane case. Experiments also show the overall trend of increasing friction when going over an edge versus a basal plane. High resolution FFM was performed using a sharp diamond tip on a native oxidized MoS_2 edge, exhibiting 3 times the increase in friction from 0.4±0.2nN at the basal plane to 1.1±0.1nN over the expose edge (Supporting information; Figure S7).

Note that, while the experimental results show the same overall trend as the simulations, it can be difficult to quantitatively compare values. The tip utilized for the DFT simulations was cut to form a 5 nm radius hemisphere, while the actual contact between the two surfaces was localized to the scale of angstroms due to system size constraints and essentially led to a flat tip surface. On the other hand, for experiments, the diamond tip radius was much larger (indirectly measured to be ~ 40 nm using the lateral peak width technique[52]). Hence, the contact area was much larger and was affected by tip shape. The tip also moved across a non-perfect surface where the interaction could be affected by variation in topography, defects, substrate effects and environmental effects (especially humidity which could not be completely removed experimentally). The DFT simulations mainly capture electronic interaction effects and are generally only useful for comparative trends within the same simulation conditions. They looked at the specific case of laterally moving a tip surface while only oxygen content was varied (this isolation of a specific variable is not easily achieved in experiments, for example a pristine unoxidized edge was not available to be measured).

Figure 5a shows the charge (electron) density for a cross-section of the pristine MoS_2 basal plane with the diamond tip over it, where the structure of the MoS_2 with Mo atoms in center (and with the highest charge concentration) sandwiched by S atoms is clearly visible. The scale $\Delta n(r)$ represents change in charge density compared to a region of no charge (shown by red). A continuous region of similar charge density extends between surface S atoms in contact with diamond tip C atoms within the same contour of charge. In contrast, for the oxidized basal plane in Figure 5b, there is a lower region of charge density present between the surface O atoms and tip atoms. The O atoms can be seen to be more electronegative than S; i.e. they have a greater concentration of charge and have pulled more charge from the nearest Mo atom than S atoms do. The region of relatively greater charge density between the tip and pristine surface S atoms likely leads to a more stable system and also allows for easier sliding of the tip as there is relatively less variation in charge as the tip travels. On the other hand, for the oxidized plane, the lowered interfacial charge density between the tip and surface O atoms likely leads to a less favorable system and the increased localization of charge also causes more drastic variations in charge as the tip travels; this would lead to greater energy variations and more resistance to sliding. A decrease in the uniformity of charge density at the surface has also been previously suggested to increase friction.[53–55]

Summary & Conclusions

In this work, the separate role of water and oxidation on the tribological behavior of ultrathin-MoS_2 (few layers of 2D-MoS_2) was investigated and compared to ultrathin-graphene. Water adsorption studies illustrated a similar behavior for pristine-MoS_2 and graphene, where a single layer of water adsorbs on the top MoS_2 surface without intercalating between the layers. The similar adsorption behavior herein was attributed to the atomic structure of these ultrathin 2D materials. XPS confirmed the presence of some oxygen on MoS_2, where exposure to the environment oxidized the reactive edges/defects site. This behavior was further supported by our DFT results, which showed that oxidation of MoS_2 edge through substitution of sulfur atoms is highly energetically favorable. Annealing MoS_2 in

air at 290°C enhanced oxygen substitution on MoS_2, increasing the oxygen content from 3.9at% to 9.6at% along the basal plane.

The role of water was studied by comparing the friction and adhesion behavior of SiO_2/MoS_2 with SiO_2/graphene, the study demonstrates that pristine-MoS_2 (few layers) is more sensitive to the presence of water. MoS_2 was observed to retain its low friction and adhesion behavior only within a low humidity regime and for a shorter humidity range (*RH*5-20%) as compared to graphene (*RH*5-50%). Water adsorption was identified as the primary mechanism dictating the tribological behavior for pristine-MoS_2 and graphene against the SiO_2 counter surfaces (SiO_2/MoS_2 and SiO_2/graphene). This also highlights that even though the same mechanism of water adsorption is the dominant factor on MoS_2 and graphene, small changes in 2D material-water interaction can significantly influence the tribological behavior and their sensitivity to water.

The role of oxidation was studied by comparing ultrathin-MoS_2 and oxidized ultrathin-MoS_2 at varying humidity to deconvolute the role of water before and after oxidation. It was found that oxidation of MoS_2 along the basal plane significantly increases the average friction as well as increases the sensitivity to water. Pristine-MoS_2 itself remains in a relatively lubricious state regardless of the humidity, and only upon increased oxidation does the observed behavior change drastically where water begins to play a more detrimental role. This was confirmed via DFT simulations which predicted an increase in friction for surface and edge oxidation. The DFT studies showed that the substitution of sulfur atoms with oxygen atoms can increase the resistance to sliding along the basal plane and over the edge. The maximum relative energy change as the tip moved across the surface increased by ~66% upon oxidation for the basal plane and the barrier for moving over the edge increased by 25% at the native oxidized edges. Charge density simulations suggest this occurs because of oxygen's more electronegative nature which causes stronger localization of charge at the surface and hence more uneven electron and energy interactions at the surface as the tip moves across it. Both DFT and experimental results suggest

that oxidation on the basal plane is more detrimental to the lubriciousness of MoS_2 than oxidation at the edges alone. This work suggests there is a threshold limit in terms of controlling humidity to be lower than *RH*20% around contacts/interfaces composed of MoS_2 to maintain a low friction regime. Sliding contacts/interfaces should be designed such that the oxidation on the basal plane surface be minimized as it is proven to be more detrimental to the behavior of MoS_2 than native oxidized edge alone. Lastly, the oxidation findings on ultrathin MoS_2 can provide insights into the behavior of microscopic MoS_2 coatings which are known to undergo re-crystallization towards well oriented planer layers.

Materials and Methods

Experimental

Sample preparation and material characterization. An extra large MoS_2 crystal (Graphene Supermarket) of >99% purity was used to fabricate the samples. Ultrathin-MoS_2 (5-8 layers of 2D MoS_2) samples were prepared by mechanical exfoliation using scotch tape onto a silicon wafer. An n-doped silicon wafer was used as a substrate which was cleaned using ethanol and methanol in an ultrasonic bath for 10 min. XPS characterization was performed on thick MoS_2 using the ESCALAB 250Xi to track the oxygen state, which uses an Al K alpha gun source (Supporting information; Figure S1). To oxidize MoS_2, Samples were annealed at 290C for 3hrs while exposed to air in a Cole Parmer Sabletemp vacuum oven (model 281A)**.** Raman spectroscopy was performed on a Bruker Senterra dispersive microscope using a 532nm laser. (Supporting information; Figure S8).

AFM calibration and measurements. All AFM experiments were performed on the Asylum Research MFP 3D AFM. Custom built AFM cantilevers were used for friction and adhesion experiments. Silica spherical beads (Polyscience Inc.) were cleaned in an ultrasonic bath using ethanol and methanol for 10 mins. The clean beads were then attached to tipless silicon cantilevers (APPNano) with epoxy using a micromanipulator-microscope setup. Using SEM (Hitachi SU3500), the bead diameter was measured

(~14 μm). The cantilever was calibrated normally and laterally, where the normal deflection sensitivity was obtained by deflecting the tip against a clean silicon wafer to obtain the slope of the normal voltage-displacement curve. The lateral deflection sensitivity was acquired by laterally deflecting against a cleaved potassium bromide (KBr) surface using the test probe method[56]. The normal and torsional stiffness of the cantilever was calibrated using Saders methods[57,58], giving a normal stiffness of 6.42 N/m. FFM was performed by scanning the probe at 90° scan angle against the sample surface, line by line at the scan rate of ~5μm/s. The AFM tip scanned forward (trace) and backward (retrace) for each scan line, where the friction force is calculated as half the difference between trace and retrace. To convert the lateral voltage to lateral force, trace and retrace voltage signals were multiplied by lateral sensitivity, torsional stiffness, and $1/h^2$, where h is the height of the AFM tip. Adhesion experiments were performed with a maximum normal load of 800nN with the dwell time of 1s. Thickness measurements were performed using tapping mode AFM imaging of MoS_2 using sharp silicon cantilever (Nanoworld) of 42 N/m stiffness and 320 kHz resonance frequency. The thickness of MoS_2 in Figure 1 were measured relative to the silicon substrate using a similar protocol reported in the literature [15,40]. The topography data points for MoS_2 and the silicon substrate were fit using a Gaussian distribution, where the difference in the mean represented the thickness.

Humidity Control. To conduct humidity dependent experiments, a custom built humidity box was used, which allowed for the control of humidity around the contact while continuously monitoring using an embedded humidity sensor (Honeywell HIH 4000). The desired humidity was maintained by controlling the ratio of wet and dry nitrogen gas of 99.9% purity into the humidity box. Wet nitrogen gas was obtained by passing the gas into a water bubbler. Experiments were initiated using new samples placed within the humidity box and purging of N_2 gas. The desired environment was allowed to stabilize before conducting experiments to ensure there was minimal drift.

Density Functional Theory. The simulations were performed using plane wave based DFT as implemented in the Quantum Espresso software package.[59] Interactions between the valence electrons and the ionic core were represented by the projector augmented wave (PAW)[60] method with Perdew-Burke-Ernzerhof (PBE) formulation.[61] Kinetic energy cutoffs of 680 eV (50 Ry) and 5578 eV (410 Ry) were used for the wave functions and the charge density, respectively. Brillouin zone integrations were performed over the Γ point and all calculations were non spin polarized. A vacuum layer of 15 Å, based on iterative testing, was added to avoid interaction between periodic surface images. Details of the system geometries are given in supporting information (Supporting information; Figure S6).

Associated Content: Complementary experimental and DFT studies are reported in the supporting information.

Author Information

Corresponding Authors:

*E-mail: filleter@mie.utoronto.ca.,

*E-mail: chandraveer.singh@utoronto.ca.

Author Contributions:

§T.A, and S.Y. contributed equally

Acknowledgments: The authors acknowledge financial support from the Ontario Ministry of Research and Innovation Early Researcher Award; the Erwin Edward Hart Endowed Professorship; the Natural Sciences and Engineering Research Council of Canada (NSERC); and the Canada Foundation for Innovation (CFI). SEM analysis was carried out at Ontario Center for the Characterization of Advanced Materials (OCCAM). The authors would also like to acknowledge B. Hatton, R. Sodhi and P. M. Sudeep for assistance with WCA measurements, XPS measurements, and Raman measurements respectively.

Reference

[1] K. Holmberg, A. Erdemir, *Friction* **2017**, *5*, 263.

[2] J. Y. Park, M. Salmeron, *Chem. Rev.* **2014**, *114*, 677.

[3] R. J. Cannara, *Director* **2009**, *780*, 780.

[4] J. R. Lince, S. H. Loewenthal, C. S. Clark, *Proc. 43rd Aerosp. Mech. Symp. NASA Ames Res. Cent.* **2016**, 221.

[5] A. S. Gibson, A. McColgan, J. C. Heald, E. Harpell, M. J. Anderson, R. Sharma, *Conf. Proc. 15th Eur. Sp. Mech. Tribol. Symp.* **2013**, 25.

[6] A. A. Voevodin, J. P. O'Neill, J. S. Zabinski, *Surf. Coatings Technol.* **1999**, *116–119*, 36.

[7] C. Donnet, J. M. Martin, T. Le Mogne, M. Belin, *Tribol. Ser.* **1994**, *27*, 277.

[8] R. H. Savage, *J. Appl. Phys.* **1948**, *19*, 1.

[9] T. W. Scharf, S. V. Prasad, *J. Mater. Sci.* **2013**, *48*, 511.

[10] R. H. Savage, D. L. Schaefer, *J. Appl. Phys.* **1956**, *27*, 136.

[11] J. F. Curry, M. A. Wilson, H. S. Luftman, N. C. Strandwitz, N. Argibay, M. Chandross, M. A. Sidebottom, B. A. Krick, *ACS Appl. Mater. Interfaces* **2017**, acsami.7b06917.

[12] C. Muratore, A. A. Voevodin, *Thin Solid Films* **2009**, *517*, 5605.

[13] K. J. Wahl, D. N. Dunn, I. L. Singer, *Wear* **1999**, *230*, 175.

[14] G. Colas, A. Saulot, E. Regis, Y. Berthier, *Wear* **2015**, *330–331*, 448.

[15] T. Arif, G. Colas, T. Filleter, *ACS Appl. Mater. Interfaces* **2018**, *10*, 22537.

[16] M. Daly, C. Cao, H. Sun, Y. Sun, T. Filleter, C. V. Singh, *ACS Nano* **2016**, acsnano.5b05771.

[17] S. Li, Q. Li, R. W. Carpick, P. Gumbsch, X. Z. Liu, X. Ding, J. Sun, J. Li, *Nature* **2016**, *539*, 541.

[18] T. Filleter, J. L. McChesney, A. Bostwick, E. Rotenberg, K. V. Emtsev, T. Seyller, K. Horn, R. Bennewitz, *Phys. Rev. Lett.* **2009**, *102*, 1.

[19] Z. Ye, A. Martini, *Appl. Phys. Lett.* **2015**, *106*, DOI 10.1063/1.4922485.

[20] K. Hasz, Z. Ye, A. Martini, R. W. Carpick, *Phys. Rev. Mater.* **2018**, *2*, 1.

[21] N. V. Medhekar, A. Ramasubramaniam, R. S. Ruoff, V. B. Shenoy, *ACS Nano* **2010**, *4*, 2300.

[22] O. C. Compton, S. W. Cranford, K. W. Putz, Z. An, L. C. Brinson, M. J. Buehler, S. T. Nguyen, *ACS Nano* **2012**, *6*, 2008.

[23] P. Egberts, Z. Ye, X. Z. Liu, Y. Dong, A. Martini, R. W. Carpick, *Phys. Rev. B - Condens. Matter Mater. Phys.* **2013**, *88*, 1.

[24] Z. Ye, P. Egberts, G. H. Han, A. T. C. Johnson, R. W. Carpick, A. Martini, *ACS Nano* **2016**, *10*, 5161.

[25] C. Lee, Q. Li, W. Kalb, X.-Z. Liu, H. Berger, R. W. Carpick, J. Hone, *Science (80-.).* **2010**, *328*, 76.

[26] Q. Li, C. Lee, R. W. Carpick, J. Hone, *Phys. Status Solidi Basic Res.* **2010**, *247*, 2909.

[27] O. Y. Fajardo, J. J. Mazo, *Phys. Rev. B - Condens. Matter Mater. Phys.* **2010**, *82*, 1.

[28] C. Greiner, J. R. Felts, Z. Dai, W. P. King, R. W. Carpick, *Nano Lett.* **2010**, *10*, 4640.

[29] M. Chhowalla, H. S. Shin, G. Eda, L. J. Li, K. P. Loh, H. Zhang, *Nat. Chem.* **2013**, *5*, 263.

[30] H. Li, J. Wang, S. Gao, Q. Chen, L. Peng, K. Liu, X. Wei, *Adv. Mater.* **2017**, *29*, 2.

[31] X. Zhao, S. S. Perry, *ACS Appl. Mater. Interfaces* **2010**, *2*, 1444.

[32] C. Lee, Q. Li, W. Kalb, X. Z. Liu, H. Berger, R. W. Carpick, J. Hone, *Science (80-.).* **2010**, *328*, 76.

[33] H. Lee, H. Jeong, J. Suh, W. H. Doh, J. Baik, H.-J. Shin, J.-H. Ko, J. Wu, Y.-H. Kim, J. Y. Park, *J. Phys. Chem. C* **2019**, DOI 10.1021/acs.jpcc.8b11426.

[34] H. Lee, J. H. Ko, J. S. Choi, J. H. Hwang, Y. H. Kim, M. Salmeron, J. Y. Park, *J. Phys. Chem. Lett.* **2017**, *8*, 3482.

[35] G. Levita, P. Restuccia, M. C. Righi, *Carbon N. Y.* **2016**, *107*, 878.

[36] K. K. Ghuman, S. Yadav, C. V. Singh, *J. Phys. Chem. C* **2015**, *119*, 6518.

[37] T. Liang, W. G. Sawyer, S. S. Perry, S. B. Sinnott, S. R. Phillpot, **2008**, 1.

[38] T. Liang, W. G. Sawyer, S. S. Perry, S. B. Sinnott, S. R. Phillpot, *J. Phys. Chem. C* **2011**, *115*, 10606.

[39] P. K. Chow, E. Singh, B. C. Viana, J. Gao, J. Luo, J. Li, Z. Lin, A. L. Elías, Y. Shi, Z. Wang, M. Terrones, N. Koratkar, *ACS Nano* **2015**, 3023.

[40] B. Rezania, N. Severin, A. V. Talyzin, J. P. Rabe, *Nano Lett.* **2014**, *14*, 3993.

[41] S. Singla, E. Anim-Danso, A. E. Islam, Y. Ngo, S. S. Kim, R. R. Naik, A. Dhinojwala, *ACS Nano* **2017**, *11*, 4899.

[42] A. P. S. Gaur, S. Sahoo, M. Ahmadi, S. P. Dash, M. J. F. Guinel, R. S. Katiyar, *Nano Lett.* **2014**, *14*, 4314.

[43] A. Kozbial, X. Gong, H. Liu, L. Li, *Langmuir* **2015**, *31*, 8429.

[44] B. Luan, R. Zhou, *Appl. Phys. Lett.* **2016**, *108*, DOI 10.1063/1.4944840.

[45] D. Ortiz-Young, H.-C. Chiu, S. Kim, K. Voïtchovsky, E. Riedo, *Nat. Commun.* **2013**, *4*, 2482.

[46] G. Tocci, L. Joly, A. Michaelides, *Nano Lett.* **2014**, *14*, 6872.

[47] P. K. Chow, E. Singh, B. C. Viana, J. Gao, J. Luo, J. Li, Z. Lin, A. L. Elías, Y. Shi, Z. Wang, M. Terrones, N. Koratkar, *ACS Nano* **2015**, *9*, 3023.

[48] M. Reguzzoni, A. Fasolino, E. Molinari, M. C. Righi, *Phys. Rev. B - Condens. Matter Mater. Phys.* **2012**, *86*, 1.

[49] G. Levita, A. Cavaleiro, E. Molinari, T. Polcar, M. C. Righi, *J. Phys. Chem. C* **2014**, *118*, 13809.

[50] J. Martincová, M. Otyepka, P. Lazar, *Chem. - A Eur. J.* **2017**, *23*, 13233.

[51] Z. Ye, A. Otero-De-La-Roza, E. R. Johnson, A. Martini, *Appl. Phys. Lett.* **2013**, *103*, DOI 10.1063/1.4818258.

[52] Y. Dong, X. Z. Liu, P. Egberts, Z. Ye, R. W. Carpick, A. Martini, *Tribol. Lett.* **2013**, *50*, 49.

[53] L. Wang, X. Zhou, T. Ma, D. Liu, L. Gao, X. Li, J. Zhang, Y. Hu, H. Wang, Y. Dai, J. Luo, *Nanoscale* **2017**, *9*, 10846.

[54] Q. Li, X. Z. Liu, S. P. Kim, V. B. Shenoy, P. E. Sheehan, J. T. Robinson, R. W. Carpick, *Nano Lett.* **2014**, *14*, 5212.

[55] J. Wang, J. Li, L. Fang, Q. Sun, Y. Jia, *Tribol. Lett.* **2014**, *55*, 405.

[56] R. J. Cannara, M. Eglin, R. W. Carpick, *Rev. Sci. Instrum.* **2006**, *77*, 53701.

[57] J. E. Sader, J. W. M. Chon, P. Mulvaney, *Rev. Sci. Instrum.* **1999**, *70*, 3967.

[58] C. P. Green, H. Lioe, J. P. Cleveland, R. Proksch, P. Mulvaney, J. E. Sader, *Rev. Sci. Instrum.* **2004**, *75*, 1988.

[59] P. Giannozzi, S. Baroni, N. Bonini, M. Calandra, R. Car, C. Cavazzoni, D. Ceresoli, G. L. Chiarotti, M. Cococcioni, I. Dabo, A. D. Corso1, S. de Gironcol, S. Fabris, G. Fratesi, R. Gebauer, U. Gerstmann, C. Gougoussis, A. Kokalj, M. Lazzeri, L. Martin-Samos, N. Marzari, F. Mauri, R. Mazzarello, S. Paolini, A. Pasquarello, L. Paulatto1, C. Sbraccia, S. Scandolo, G. Sclauzero, A. P. Seitsonen, A. Smogunov, P. U. Renata M Wentzcovitch, *J. Phys. Condens. Matter* **2009**, *21*, DOI 10.1088/0953-8984/21/39/395502.

[60] G. Kresse, D. Joubert, *Phys. Rev. B* **1999**, *59*, 11.

[61] J. P. Perdew, K. Burke, M. Ernzerhof, *Phys. Rev. Lett.* **1996**, *77*, 3865.

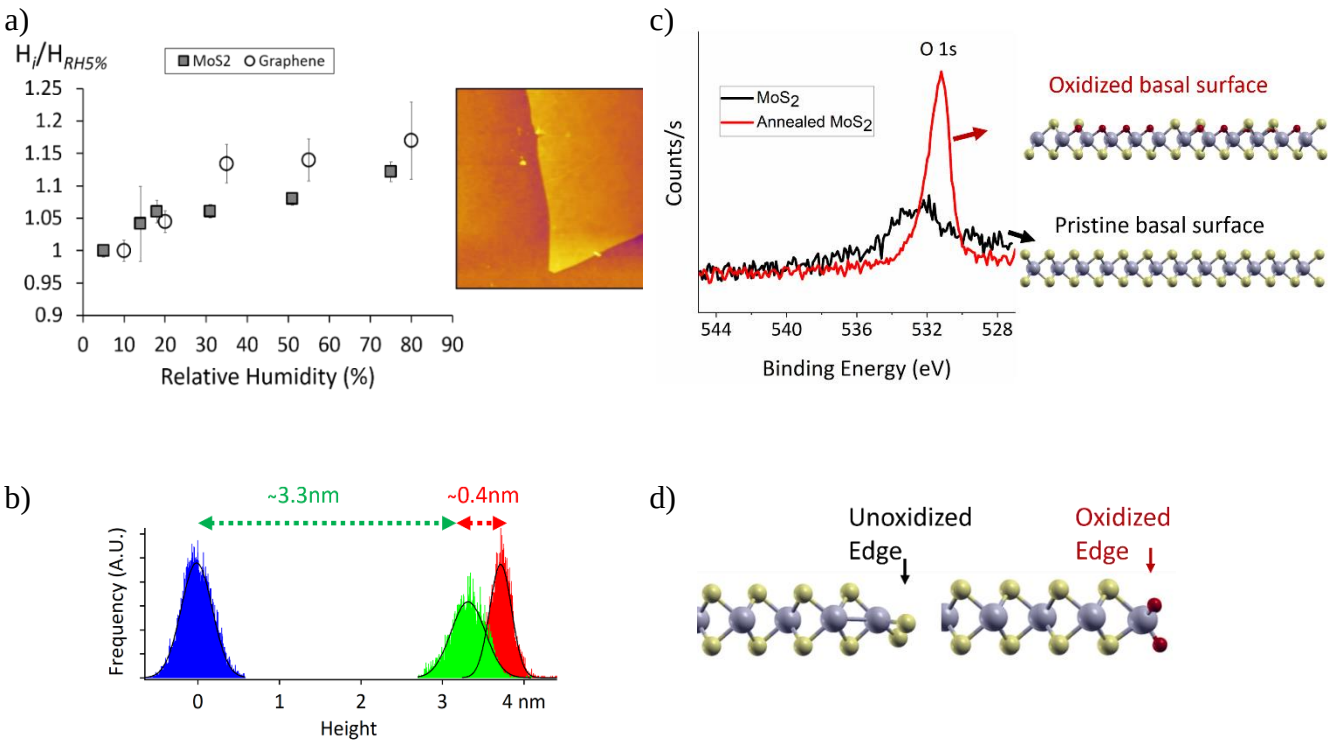

Figure 1: a) Normalized thickness of pristine ultrathin-MoS_2 as a function of humidity. Inset: Tapping mode image (2x2 μm) of MoS_2 topography (Change in thickness of graphene is replotted from published work to help compare the behavior[15]). b) pristine-MoS_2 thickness at *RH*5% (green) and *RH*75% (red) relative to the silicon wafer (blue). c) High-resolution XPS of O1s oxygen peak for MoS_2 and annealed MoS_2. Insets: DFT simulation models of pristine and oxidized MoS_2 basal planes. d) DFT models of pristine (unoxidized) and oxidized MoS_2 edges.

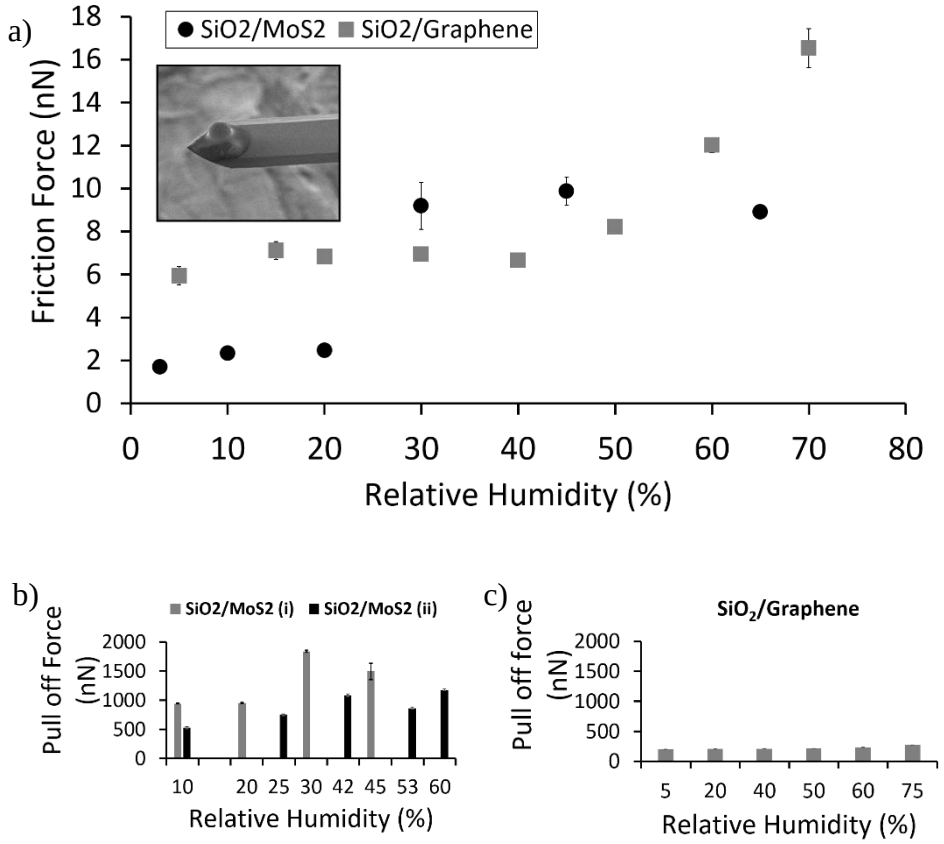

Figure 2: a) Comparison of average friction force between a beaded SiO_2 tip against pristine-MoS_2 and graphene with 20nN normal load as a function of relative humidity. Any error bars not visible are smaller than the size of the data point marker. Top-left inset: SEM of SiO_2 beaded tip. b) Adhesion between SiO_2/ pristine-MoS_2 interface as a function of humidity. c) Adhesion between SiO_2/graphene interface as a function of humidity. (Friction and adhesion of SiO_2/graphene is reproduced here from our earlier published work[15])

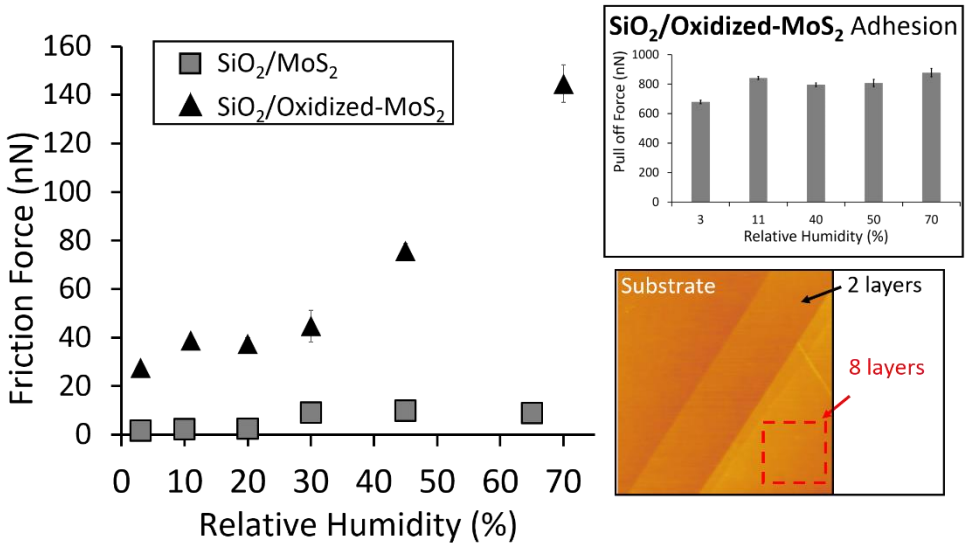

Figure 3: Comparison of average friction force between beaded SiO_2 tip against pristine-MoS_2 and oxidized-MoS_2 at 20nN normal load as a function of relative humidity. Any error bars not visible are smaller than the size of the data point marker. Top-right inset: Adhesion trend between SiO_2/oxidized-MoS_2 interface as a function of humidity. Bottom-left inset: Topography image of oxidized MoS_2 (15x15μm). The dashed box (red) indicates the area of interest for FFM.

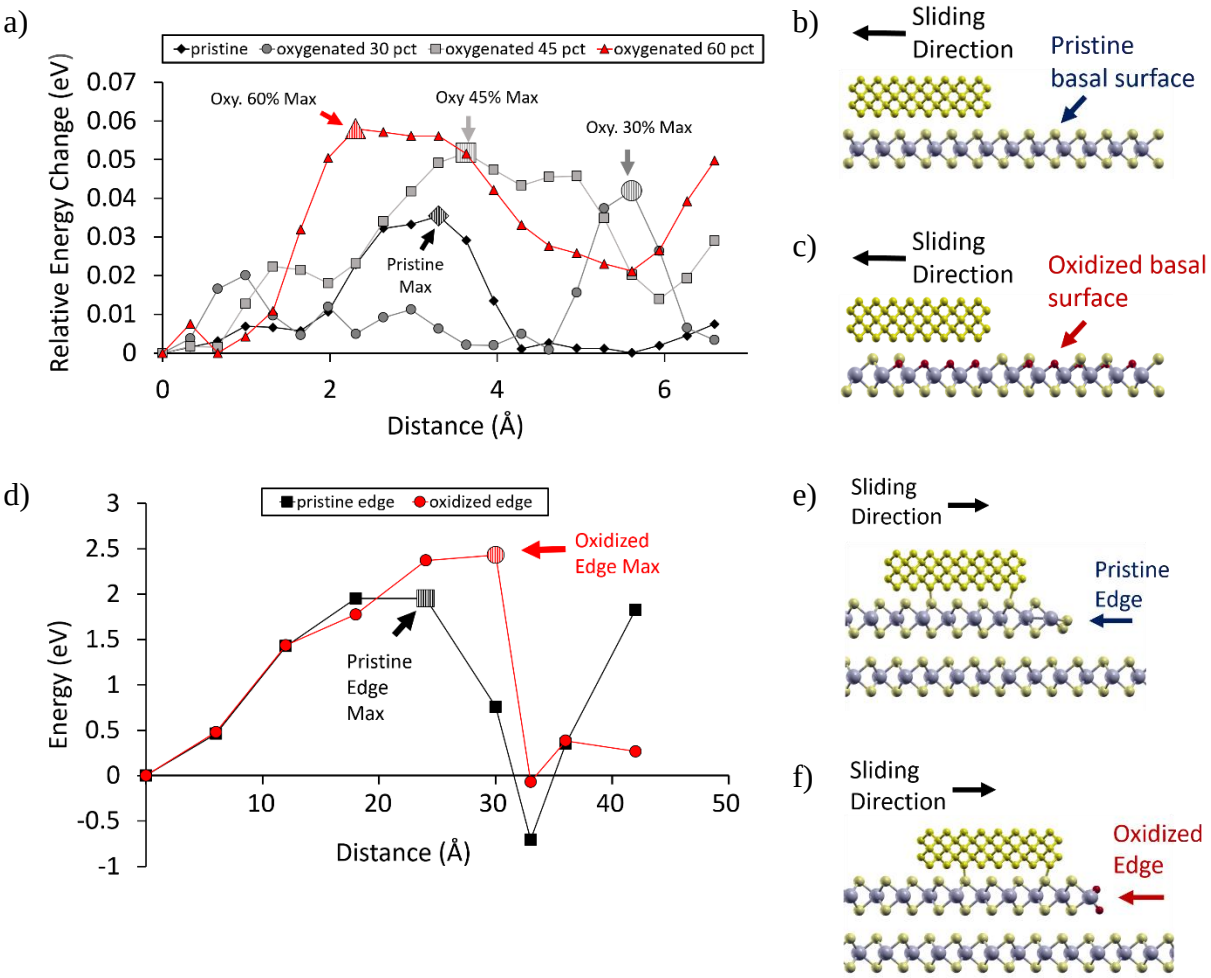

Figure 4: a) DFT based comparison of diamond tip interaction tracking the relative energy change as tip is moved on basal planes with increasing oxygen content in the top layer of sulfur atoms. b-c) DFT model of pristine and 60% oxygen covered MoS2 basal plane with sliding diamond tip. c) DFT model of 60% oxygen covered MoS2 basal plane with sliding diamond tip. d): Energy profile as tip is moved towards and over a pristine and oxidized edge. e-f) DFT model of pristine and oxidized MoS_2 step edge with sliding diamond tip.

a)

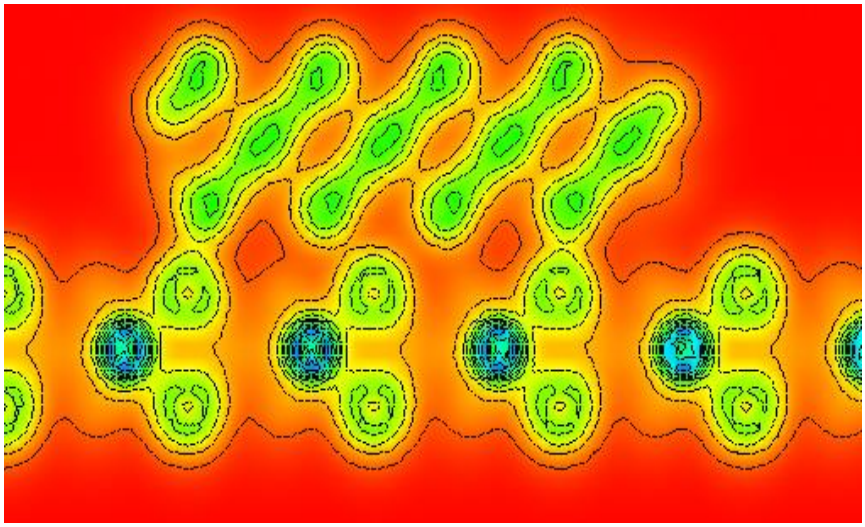

b)

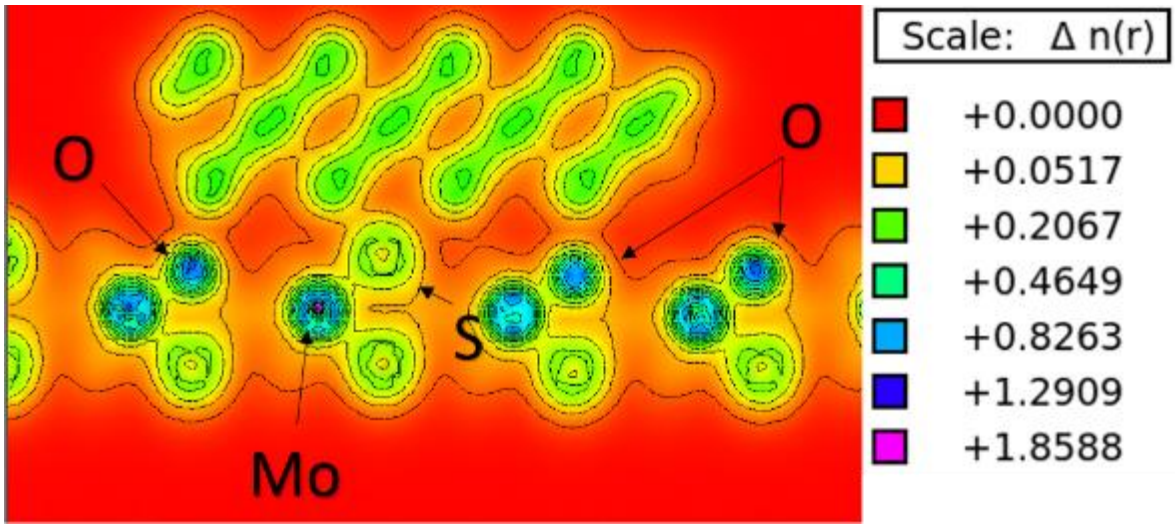

Figure 5: Charge density of a) Pristine MoS_2 and Oxidized MoS_2 against a diamond tip counter surface. The scale Δn(r) represents change in charge density compared to a region of no charge (shown by red).

Table 1: Experimental-computational comparison of friction for oxidized MoS2. Left: Sample configurations. Middle: The maximum energy changes for different MoS_2 surfaces as a diamond tip was translated using DFT. Higher energy changes correspond to greater friction force. Right: AFM friction measurements on MoS_2 and oxidized MoS_2 along the basal plane and edge using SiO_2 and diamond tips.

Surface	**DFT maximum energy change [eV]**	**Experimental friction [nN] – at *RH*3-5%**
	Basal Planes	
Pristine	0.035	1.7±0.1nN [SiO_2 sphere tip] 0.4±0.2nN [Diamond sharp tip]
30% oxygen coverage (9.7at%)	0.042	27±1.3 nN [SiO_2 sphere tip]
45% oxygen coverage (15.3at%)	0.052	-
60% oxygen coverage (19.4at%)	0.058	-
	Step Edges	
Pristine	1.952	-
Oxidized	2.432	1.1nN ± 0.1nN [Diamond sharp tip]

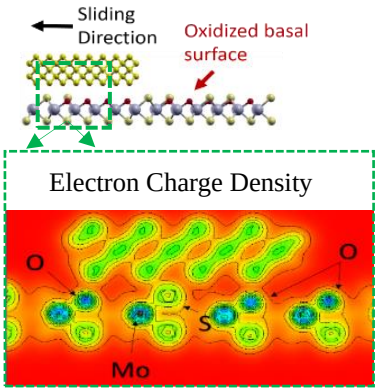

TOC: Electron charge density of the tip/oxidized-MoS2 interface showing the localized and non-uniform interfacial charge distribution on oxygen rich MoS_2 leads to higher resistance to sliding.